A Robust Attitude Tracking Controller for Spacecraft Based on Singularity-Free Quaternion Nonlinear Dynamic Inversion Framework

Chang-Te Shen , Ciann-Dong Yang * , Yei-Chin Chao *

Posted Date: 29 April 2026

doi: 10.20944/preprints202604.2045.v1

Keywords: quaternions; nonlinear dynamic inversion; disturbance observer-based controller; spacecraft attitude control

 doi:10.20944/preprints202604.2045.v1

Article

A Robust Attitude Tracking Controller for Spacecraft Based on Singularity-Free Quaternion Nonlinear Dynamic Inversion Framework

Chang-Te Shen, Ciann-Dong Yang * and Yei-Chin Chao *

Department of Aeronautics and Astronautics, National Cheng Kung University, Taiwan

* Correspondence: cdyang@mail.ncku.edu.tw; ycchao@mail.ncku.edu.tw

Abstract

This paper presents a robust linear-quadratic attitude-tracking controller for a nonlinear spacecraft with disturbances. Quaternions are used to represent the spacecraft's attitude to prevent gimbal lock associated with Euler angles. Nonlinear rotation dynamics are controlled by nonlinear dynamic inversion (NDI) with an augmented linear-quadratic controller. However, quaternions in rotation dynamics can encounter singularities during dynamic inversion, leading to numerical instability in control input calculations. To resolve this problem, we propose a new NDI method based on the Lagrange equation for quaternion dynamics. Since NDI may not fully compensate for nonlinearities due to unknown disturbances or modeling errors, a nonlinear disturbance observer is incorporated into the controller to compensate for disturbances. Simulations are performed to compare with previous work and according to a real attitude control testbed with gravity disturbances. Validation results demonstrate strong disturbance rejection and singularity-free performance for the proposed controller framework.

Keywords: quaternions; nonlinear dynamic inversion; disturbance observer-based controller; spacecraft attitude control

1. Introduction

The control of spacecraft attitude has evolved significantly, progressing from classical linear techniques to advanced nonlinear architectures capable of meeting the rigorous agility requirements of modern missions. Conventional Proportional-Integral-Derivative (PID) controllers have served as the industry standard due to their implementation simplicity and extensive flight heritage. While effective for set-point regulation, PID designs often struggle with the strong gyroscopic coupling encountered during rapid, large-angle maneuvers. Some researchers have proposed modified PID methods to increase robustness and overcome the phenomenon [1–3]. To address the multi-variable interactions, Linear Quadratic Regulator (LQR) was introduced, providing a systematic framework for minimizing energy and error for multi-input-multi-output (MIMO) systems [4–7]. However, both PID and LQR are inherently limited by their linearization around equilibrium points and often need extensive gain scheduling to cover the full flight envelope. To bridge this gap, Linear-Parameter-Varying (LPV) control has emerged as a powerful intermediate solution [8,9], allowing designers to embed nonlinear dynamics into a family of linear models scheduled by state-dependent parameters, thus extending the valid operating range of linear techniques.

Despite these advancements, the nonlinearity of rigid body dynamics - particularly at high angular velocities - has driven research toward purely nonlinear control paradigms. Sliding Mode Control (SMC) has been widely investigated for its robust properties, utilizing discontinuous control laws to force system states onto a predefined sliding manifold [10,11]. While SMC is theoretically invariant to matched uncertainties, it famously suffers from the "chattering" phenomenon, which can excite high-frequency structural modes and wear down actuators. Another way to address the

 doi:10.20944/preprints202604.2045.v1

nonlinearity is nonlinear dynamic inversion (NDI), also known as feedback linearization, which offers a more geometric and physically intuitive alternative. Unlike robust controllers that fight against nonlinearities, NDI exploits the system's physics to cancel them. By algebraically transforming the nonlinear spacecraft dynamics into a linear time-invariant (LTI) system, NDI enables the application of well-understood linear control laws to the "synthetic" LTI system.

The NDI technique has been widely implemented in aerospace systems, from aircraft flight control [12–14], reentry vehicle [15], reusable rocket [16], and satellites [11,17,18]. A two-loop cascaded flight control architecture is commonly used for attitude control based on the assumption of time-scale separation. In this approach, the angular velocity loop (the inner loop) and the attitude loop (the outer loop) are linearized and controlled separately. This method simplifies the controller design process. Banerjee et al. [18] demonstrate the conventional two-loop structure NDI in the attitude control of a lunar lander, employing Euler angles for attitude representation. However, the use of Euler angles is hindered by a singularity at pitch angles of ±90 degrees, a phenomenon known as gimbal lock. As a result, alternative approaches for attitude representation, such as quaternions, have garnered increasing attention.

Unlike the conventional cascaded structure, we can select quaternions as the output and directly linearize them with respect to the input torque using the NDI technique. The angular velocity is implicitly dictated by the quaternion kinematics equation [11]. However, there is a dimension mismatch between the output quaternion, which is represented as a vector in $\mathbb{R}^4$, and the input torque, which is a vector in $\mathbb{R}^3$. To resolve this issue, previous studies [11,17,19,20] have used only the vector part of the quaternions as the output, while computing the scalar part using the unit-quaternion constraint. It has been noted, however, that a singularity may occur in the matrix inversion during NDI when the scalar part of the quaternions is zero, leading to numerical instability in control processes. Long et al. [19] and Navabi et al. [20] demonstrate that the internal dynamics of the linearized system remain stable as long as the scalar part of the quaternions is non-zero. To address this issue, Bang et al. [11] proposed adding a small value to the scalar part of the quaternions when it approaches zero, thus avoiding singularities. Bhargavapuri et al. [21] focused on quaternion error, defined as the difference between the desired and actual quaternions. They integrated the scalar part of the quaternions into the NDI framework to prevent it from crossing zero.

Previous research indicates that matrix inversion in NDI is related to the control input and the second derivatives of the output function in rotational dynamics. While earlier studies employed Newtonian mechanics to describe these motions, they encountered singularities with the matrix inverse. Therefore, it is worthwhile to explore alternative approaches. Udwadia et al. [22] present a direct method for obtaining Lagrange rotational motion using quaternions. This approach establishes the relationship between torque and the second derivatives of quaternions, while accounting for the unit-quaternion constraints.

In this paper, we successfully derive a quaternion-based NDI using the Lagrange equation of motion, not suffering from the singularity issues observed in previous studies. After eliminating the nonlinearity using NDI, we can implement a linear controller for the input-output linearized system. In this paper, we design a Linear Quadratic Tracking (LQ) controller that incorporates both feedback and feedforward gains to achieve the desired attitude while ensuring the stabilization of the quaternions and their derivatives. Additionally, a first-order filter is introduced before the controller to smooth the reference signal, rather than applying a step signal directly. This approach helps prevent actuator saturation.

The NDI can effectively cancel system nonlinearity, but its performance relies heavily on the accuracy of state feedback and the model information. Model discrepancies and external disturbances can impair the effectiveness of the nonlinearity cancellation. Chen and Yang [23,24] introduced a nonlinear disturbance observer-based control (DOBC) approach to improve the NDI's ability to manage disturbances and uncertainties resulting from model mismatches. The DOBC consists of two main components: disturbance estimation and compensation. Chen et al. [25] categorized various types of observers based on their application to linear or nonlinear systems, as well as the

 doi:10.20944/preprints202604.2045.v1

compensation mechanisms addressing external disturbances or model mismatches. We propose a framework for control that combines NDI with DOBC, suggesting an appropriate nonlinear observer gain derived from the quaternion NDI.

Before applying the control algorithm to a mission, it is beneficial to verify it using a ground attitude control testbed. We developed this testbed based on a spherical air-bearing [26] to provide frictionless rotation, simulating the in-orbit environment. The testbed is powered by hydrogen peroxide thrusters, which can deliver 5.25 Nm of torque on each rotational axis. The testbed is developed to validate the feasibility of the NDI-DOBC framework. Because there is a displacement between the center of gravity of the testbed and the center of the spherical air-bearing, gravity contributes a disturbance torque that depends on the attitude. This makes the DOBC crucial for disturbance cancellation and enhances overall control performance. The simulations demonstrate the effectiveness of the proposed quaternion-based NDI method, highlighting its singularity-free properties in comparison to previous approaches. Additional simulations utilize the model of our attitude control testbed to showcase the control capabilities and disturbance rejection abilities of the NDI-DOBC framework.

This paper is organized as follows: Section II presents the schematic of the entire NDI-DOBC framework and introduces the attitude control testbed. Section III discusses the Lagrange equation of rotational motion based on quaternions. Section IV derives the quaternion NDI and proves its singularity-free property. Additionally, a linear-quadratic tracking controller is designed based on the linearized system. In Section V, we adopt a DOBC framework for disturbance estimation and cancellation to design a nonlinear observer gain with reference to our quaternion NDI. Section VI presents four case studies of simulation results that demonstrate the performance and capabilities of our work. Finally, Section VII concludes the paper.

2. System Architecture

This section introduces the schematic of the NDI-DOBC architecture and the attitude control testbed. First, we present a system overview in the form of a block diagram, providing a visual summary of the framework.

2.1. System Block Diagram

The NDI-DOBC block diagram is shown in Figure 1. For clarity, we delineate the signal propagation from the reference input to the system output. The design process is divided into signal filtering, linear quadratic (LQ) tracking control, nonlinear-dynamic-inversion (NDI) linearization, and disturbance observation. This graphical mapping connects the general overview to each subsystem described below.

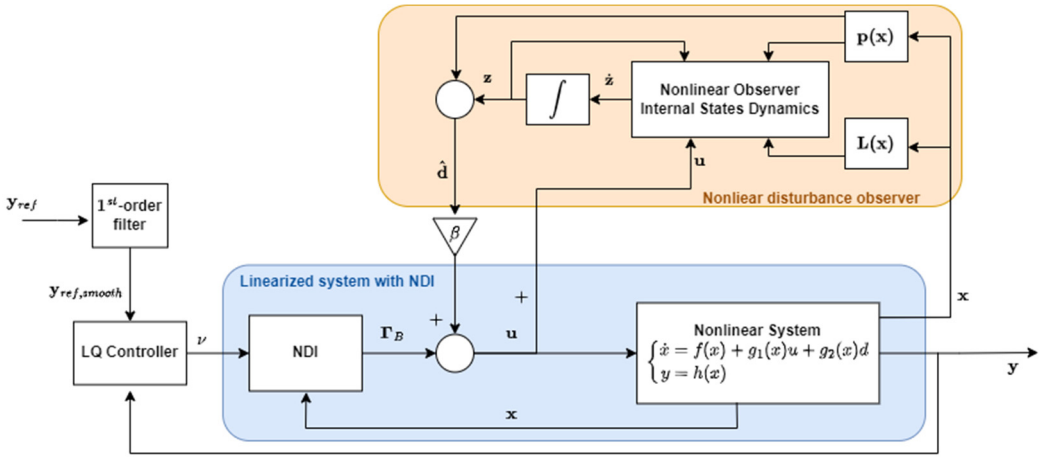

Figure 1. Block diagram of the NDI-DOBC framework for attitude tracking control. The system consists of three parts: 1. The NDI linearized system in the blue block; 2. The nonlinear disturbance observer (orange block),

 doi:10.20944/preprints202604.2045.v1

which estimates external disturbances and computes the disturbance compensation term by multiplying it by the compensation gain beta; 3. An LQ controller and a filter to control the linearized system.

A first-order filter, acting as a signal smoother, is placed before the controller to smooth the input signal. For a large-angle maneuver, this smoother outputs a continuous curve to the controller instead of a step function. This prevents excitation of the nonlinearity and actuator saturation from rapid movement. The linear-quadratic tracking controller is designed using the linearized system. It stabilizes the system with state-feedback gains and provides feed-forward gains to improve tracking accuracy. The outputs of the LQ tracking controller, known as "virtual inputs," serve as the inputs to the linearized system. The NDI then converts these "virtual inputs" into real, physically meaningful control torques for rotational motion.

The disturbance observer, shown as an orange block, estimates external disturbance using information from the original nonlinear system. The nonlinear function $\boldsymbol{p}(\boldsymbol{x})$ and the observer gain $\boldsymbol{L}(\boldsymbol{x})$ are to be designed to ensure the disturbance estimate error stays asymptotically stable regardless of the states $\boldsymbol{x}$. The estimated disturbance is then multiplied by the compensation gain $\boldsymbol{\beta}$ and added to the NDI control torques. These serve as inputs to the nonlinear system. Details are given in Section IV.

2.2. Attitude Control Testbed

The attitude control testbed consists of a circular plate with eight thrusters that produce torques around the yaw, pitch, and roll axes. The plate rotates without friction on a spherical air bearing to mimic spacecraft movement. Each thruster, fueled by hydrogen peroxide and controlled by a solenoid valve, can generate up to 5.25 Nm of torque for each axis. The onboard computer estimates the current state by combining data from the inertial measurement unit (IMU) and the ArUco marker's attitude. It also computes control commands to operate the eight solenoid valves in an on/off manner. The testbed is shown in Figure 2.

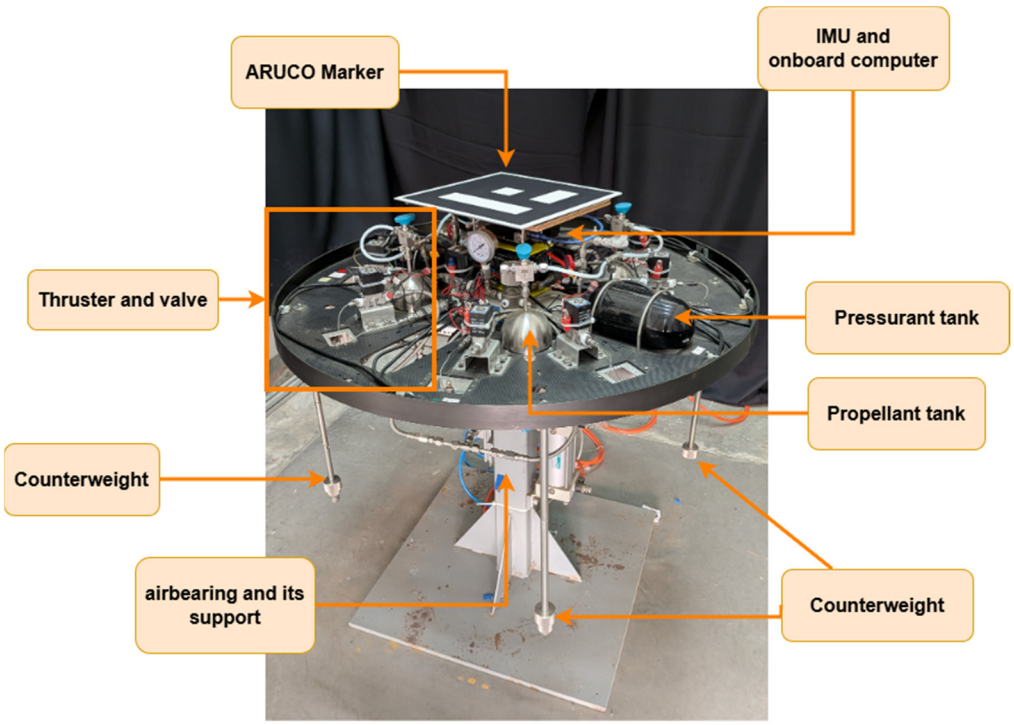

Figure 2. Attitude control testbed. The testbed is mounted on a spherical air bearing that provides frictionless rotation with three degrees of freedom. It includes eight monopropellant thrusters as actuators for attitude control. An external camera captures images of the ArUco marker, which is used to calculate the marker's attitude and is fused with the onboard IMU to determine the testbed's attitude estimate.

 doi:10.20944/preprints202604.2045.v1

The numerous components on the testbed make it difficult to align the center of gravity with the air bearing's center. This misalignment creates a lever arm, causing gravity to generate torque and disturb attitude control. Figure 3 demonstrates how gravity acts as an external disturbance that varies with roll and pitch angles. Consequently, the disturbance observer is vital for effective attitude control.

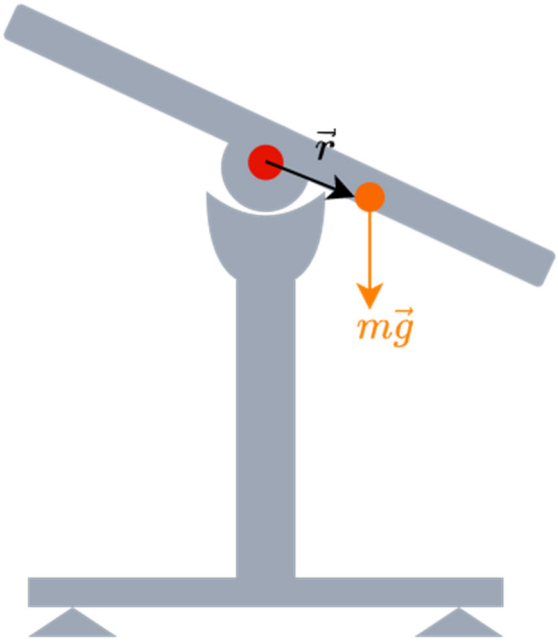

Figure 3. Illustration of the gravity disturbance acting on the attitude control testbed. The misalignment of the center of gravity and the center of air bearing causes a disturbance torque.

3. Quaternion Rotation Dynamics

This section introduces the Lagrange equation of rotational motion using quaternions, which is essential for deriving NDI in the next section. Udwadia first derived this equation in 2010 using a direct Lagrange approach without relying on the concept of Lagrange multipliers or Newtonian mechanics [22]. The derivation constructs the Lagrangian from energy terms and expresses the unconstrained equation of motion in terms of quaternions, their derivatives, angular velocity, and generalized torque. The unit-quaternion constraint is incorporated by applying the fundamental equation of constrained motion [27], resulting in a constrained equation of motion. The relationship between generalized and physical torque is then established, providing an equation that describes rotational dynamics in terms of quaternions while satisfying the unit-quaternion constraint for a given input torque.

The derivation begins with the Lagrangian, defined as kinetic energy minus potential energy. For rotational motion, only kinetic energy is present, so the Lagrangian is $T = \frac{1}{2}\boldsymbol{\omega}^T\hat{\boldsymbol{J}}\boldsymbol{\omega}$. The body-fixed coordinate axes are assumed to align with the principal axes of the rigid body, resulting in a diagonal moment of inertia matrix $\hat{\boldsymbol{J}} = diag(J_1, J_2, J_3)$. The Lagrange equation of motion is:

$$\frac{d}{dt}\left(\frac{\partial \boldsymbol{T}}{\partial \dot{\boldsymbol{q}}}\right) - \frac{\partial \boldsymbol{T}}{\partial \boldsymbol{q}} = \boldsymbol{\Gamma}_q \tag{1}$$

Equation (1) is an unconstrained equation of motion. The quaternion vector $\boldsymbol{q} = [q_0 \quad q_1 \quad q_2 \quad q_3]$ serves as the generalized coordinate, with each element considered independent. Quaternions are divided into the scalar part q_0 and the vector part $\boldsymbol{q}_v = [q_1 \quad q_2 \quad q_3]$. The input to Equation (1) is a 4×1 generalized quaternion torque vector $\boldsymbol{\Gamma}_q$. Several properties of quaternions are useful for expanding and rearranging Equation (1):

 doi:10.20944/preprints202604.2045.v1

Quaternion time derivatives: The quaternion time derivative is defined as the "quaternion product" of the quaternion and the augmented angular velocity:

$$\dot{\boldsymbol{q}} = \frac{1}{2}\boldsymbol{q} \otimes \boldsymbol{w} \tag{2}$$

Here, $\otimes$ denotes the quaternion product, and the augmented angular velocity is $\boldsymbol{w} = [0 \quad \omega_1 \quad \omega_2 \quad \omega_3]$. Using the properties of quaternions, equation (can be rearranged into two matrix forms [28]:

$$\dot{\boldsymbol{q}} = \frac{1}{2}\boldsymbol{E}^T\boldsymbol{w} \tag{3}$$

$\boldsymbol{E}$ and $\dot{\boldsymbol{E}}$ represent the orthogonal matrix of quaternions and its time derivative:

$$\boldsymbol{E} = \begin{bmatrix} q_0 & q_1 & q_2 & q_3 \\ -q_1 & q_0 & q_3 & -q_2 \\ -q_2 & -q_3 & q_0 & q_1 \\ -q_3 & q_2 & -q_1 & q_0 \end{bmatrix} = \begin{bmatrix} \boldsymbol{q}^T \\ \\ \boldsymbol{E}_1 \end{bmatrix} \tag{4}$$

From Equation (3), the augmented angular velocity can be expressed as:

$$\boldsymbol{w} = 2\boldsymbol{E}\dot{\boldsymbol{q}} \tag{5}$$

Properties of matrix $\boldsymbol{E}$ and $\boldsymbol{E}_1$: $\boldsymbol{E}_1$ is a submatrix of $\boldsymbol{E}$ shown in Equation (4). $\boldsymbol{E}$ is an orthogonal matrix, and $\boldsymbol{E}_1$ is a 3×4 matrix with orthogonal rows, hence they have the following property:

$$\boldsymbol{E}\,\boldsymbol{E}^T = \boldsymbol{I}_{4\times4} \quad , \quad \boldsymbol{E}_1\boldsymbol{E}_1^T = \boldsymbol{I}_{3\times3} \tag{6}$$

$\boldsymbol{q}$ lies in its null space because each row of $\boldsymbol{E}_1$ is orthogonal to $\boldsymbol{q}$. Multiplying $\boldsymbol{E}_1$ by the quaternion vector yields a zero vector:

$$\boldsymbol{E}_1\boldsymbol{q} = \boldsymbol{0} \tag{7}$$

From Equations (4) and (7), it follows that:

$$\boldsymbol{E}\boldsymbol{q} = \begin{bmatrix} 1 \\ 0 \\ 0 \\ 0 \end{bmatrix} \tag{8}$$

Substituting the quaternions with their time derivatives in Equation (7), the $\boldsymbol{E}_1$ matrix transforms into $\dot{\boldsymbol{E}}_1$. Each row of $\dot{\boldsymbol{E}}_1$ is orthogonal to $\dot{\boldsymbol{q}}$:

$$\dot{\boldsymbol{E}}_1\dot{\boldsymbol{q}} = \boldsymbol{0} \tag{9}$$

Equation (9) will appear later for the observer gain design.

Unit-quaternion constraint: When quaternions represent attitude, they must satisfy the unit-norm constraint: $\|\boldsymbol{q}\|_2 = 1$. This leads to the following expression:

$$N(\boldsymbol{q}) = \boldsymbol{q}^T\boldsymbol{q} = 1 \tag{10}$$

Differentiate Equation (8) with respect to time, and substitute the result $\dot{\boldsymbol{E}}\boldsymbol{q} = -\boldsymbol{E}\dot{\boldsymbol{q}}$ into Equation (5), this yields another expression of augmented angular velocity:

$$\boldsymbol{w} = -2\dot{\boldsymbol{E}}\boldsymbol{q} \tag{11}$$

Substituting Equations (5) and (11) into the kinetic energy equation, the rotational kinetic energy can be expressed in terms of quaternions and their derivatives:

$$T = \frac{1}{2}\boldsymbol{\omega}^T\hat{\boldsymbol{J}}\boldsymbol{\omega} = \frac{1}{2}\boldsymbol{w}^T\boldsymbol{J}\boldsymbol{w} = 2\dot{\boldsymbol{q}}^T\boldsymbol{E}^T\boldsymbol{J}\boldsymbol{E}\dot{\boldsymbol{q}} = 2\boldsymbol{q}^T\dot{\boldsymbol{E}}^T\boldsymbol{J}\dot{\boldsymbol{E}}\boldsymbol{q} \tag{12}$$

$\boldsymbol{J} = diag(J_0, J_1, J_2, J_3)$ is a 4×4 extended moment of inertia matrix matching the dimension of $\boldsymbol{w}$, where J_0 is an arbitrary positive number. The unconstrained Lagrange equation of motion (1) can also be rearranged as follows:

 doi:10.20944/preprints202604.2045.v1

$$4\boldsymbol{E}^T\boldsymbol{J}\dot{\boldsymbol{E}}\ddot{\boldsymbol{q}} + 8\dot{\boldsymbol{E}}^T\boldsymbol{J}\boldsymbol{E}\dot{\boldsymbol{q}} + 4J_0N(\dot{\boldsymbol{q}})\boldsymbol{q} = \boldsymbol{\Gamma}_{\boldsymbol{q}} \tag{13}$$

Applying the fundamental equation of constrained motion [27] incorporates the unit-quaternion constraint into the unconstrained system. After algebraic manipulation, the arbitrary number J_0 is eliminated, and the generalized acceleration $\ddot{\boldsymbol{q}}$ is given by Equation (13) as

$$\ddot{\boldsymbol{q}} = -\frac{1}{2}\boldsymbol{E}_1^T\hat{\boldsymbol{J}}^{-1}\boldsymbol{\omega}^{\times}\hat{\boldsymbol{J}}\boldsymbol{\omega} - N(\dot{\boldsymbol{q}})\boldsymbol{q} + \frac{\boldsymbol{E}_1^T\hat{\boldsymbol{J}}^{-1}\boldsymbol{E}_1\boldsymbol{\Gamma}_{\boldsymbol{q}}}{4} \tag{14}$$

$\boldsymbol{w}^{\times}$ in Equation (14) denotes the skew-symmetric matrix of angular velocity, defined as:

$$\boldsymbol{\omega}^{\times} = \begin{bmatrix} 0 & -\omega_3 & \omega_2 \\ \omega_3 & 0 & -\omega_1 \\ -\omega_2 & \omega_1 & 0 \end{bmatrix} \tag{15}$$

For practical applications, the generalized quaternion torque vector must be converted to a physical torque $\boldsymbol{\Gamma}_B$. Udwadia [22] established the relationship between these torques using the "virtual work method," resulting in:

$$\boldsymbol{\Gamma}_{\boldsymbol{q}} = 2\boldsymbol{E}_1^T\boldsymbol{\Gamma}_B \tag{16}$$

By substituting Equation (16) into Equation (14), the Lagrange equation of motion for rigid body rotation using quaternions and body-fixed frame torque is obtained:

$$\ddot{q} = -\frac{1}{2}\boldsymbol{E}_1^T\hat{\boldsymbol{J}}^{-1}\boldsymbol{\omega}^{\times}\hat{\boldsymbol{J}}\boldsymbol{\omega} - N(\dot{\boldsymbol{q}})\boldsymbol{q} + \frac{\boldsymbol{E}_1^T\hat{\boldsymbol{J}}^{-1}\boldsymbol{\Gamma}_B}{2} \tag{17}$$

4. Quaternion NDI and LQ Tracking Controller

In this section, we apply nonlinear dynamic inversion (NDI) to the rotational dynamics – based on the Lagrange equations of motion presented in Equation (17) – to obtain a linearized dynamic model. Following this, a linear quadratic (LQ) tracking controller is developed for the linearized system, utilizing both state feedback and feedforward gains to ensure precise tracking performance.

To simplify controller design, we linearize the output with respect to the inputs using NDI by applying the Lie derivatives to the output function. By comparing the system equations with the Lagrange equation of motion from Section 3, we define the system states. While rotation dynamics typically use attitude and angular velocity as state variables, our approach uses quaternions and their time derivatives.

Equations (3) and (17) can be rewritten as follows:

$$\dot{\boldsymbol{x}}(t) = \boldsymbol{f}(\boldsymbol{x}(t)) + \boldsymbol{g}(\boldsymbol{x}(t))\boldsymbol{u} \tag{18}$$

with the output function defined as:

$$\boldsymbol{y}(t) = \boldsymbol{h}(\boldsymbol{x}(t)) \tag{19}$$

where $\boldsymbol{x} = [\boldsymbol{q}^T \quad \dot{\boldsymbol{q}}^T]^T$. The terms $\boldsymbol{f}(\boldsymbol{x})$ and $\boldsymbol{g}(\boldsymbol{x})$ in Equation (18) are

$$\boldsymbol{f}(\boldsymbol{x}) = \begin{bmatrix} \boldsymbol{f}_u \\ \boldsymbol{f}_l \end{bmatrix} = \begin{bmatrix} \frac{1}{2}\boldsymbol{E}^T\boldsymbol{w} \\ -\frac{1}{2}\boldsymbol{E}_1^T\hat{\boldsymbol{J}}^{-1}\boldsymbol{\omega}^{\times}\hat{\boldsymbol{J}}\boldsymbol{\omega} - N(\dot{\boldsymbol{q}})\boldsymbol{q} \end{bmatrix}, \boldsymbol{g}(\boldsymbol{x}) = \begin{bmatrix} \boldsymbol{g}_u \\ \boldsymbol{g}_l \end{bmatrix} = \begin{bmatrix} \boldsymbol{0}_{4\times3} \\ \frac{1}{2}\boldsymbol{E}_1^T\hat{\boldsymbol{J}}^{-1} \end{bmatrix} \tag{20}$$

Here, the angular velocity vector $\boldsymbol{\omega}$ is treated as a parameter, with its relationship to $\dot{\boldsymbol{q}}$ given in Equation (3). If the quaternion time derivatives are bounded, the angular velocity will also remain bounded.

The control inputs are the torques applied to the body axes, $\boldsymbol{u} = \boldsymbol{\Gamma}_B$. We define the system outputs as the attitude quaternions:

$$\boldsymbol{y} = [\boldsymbol{I}_{4\times4} \quad \boldsymbol{0}_{4\times4}]\begin{bmatrix} \boldsymbol{q} \\ \dot{\boldsymbol{q}} \end{bmatrix} \tag{21}$$

 doi:10.20944/preprints202604.2045.v1

At this stage, equation (21) shows that the outputs are not directly related to the system inputs. To clarify this relationship, we recursively apply the Lie derivatives to the output vector until the system inputs appear.

$$\begin{aligned}\dot{\boldsymbol{y}} &= \frac{d\boldsymbol{y}(\boldsymbol{x}(t))}{dt} = \frac{\partial \boldsymbol{h}}{\partial \boldsymbol{x}}\frac{d\boldsymbol{x}}{dt} \\ &= \nabla \boldsymbol{h} \cdot (\boldsymbol{f} + \boldsymbol{g}\vec{\boldsymbol{u}}) = L_{\boldsymbol{f}}\boldsymbol{h}(\boldsymbol{x}) + L_{\boldsymbol{g}}\boldsymbol{h}(\boldsymbol{x})\vec{\boldsymbol{u}} \\ &= [\boldsymbol{I}_{4\times4} \quad \boldsymbol{0}_{4\times4}] \cdot \boldsymbol{f}(\boldsymbol{x}) + [\boldsymbol{I}_{4\times4} \quad \boldsymbol{0}_{4\times4}] \cdot \boldsymbol{g}(\boldsymbol{x})\boldsymbol{\Gamma}_B \\ &= \frac{1}{2}\boldsymbol{E}^T\boldsymbol{w}\end{aligned} \tag{22}$$

The time derivative of the output $\boldsymbol{y}$ indicates that the Lie derivatives $\boldsymbol{L_g h(x)}$ is zero, so we proceed to the second derivative.

$$\ddot{\boldsymbol{y}} = \frac{d}{dt}\big(L_{\boldsymbol{f}}\boldsymbol{h}(\boldsymbol{x})\big) = L_{\boldsymbol{f}}^2\boldsymbol{h}(\boldsymbol{x}) + L_{\boldsymbol{g}}L_{\boldsymbol{f}}\boldsymbol{h}(\boldsymbol{x})\boldsymbol{u} = \boldsymbol{F}(\boldsymbol{x}) + \boldsymbol{G}(\boldsymbol{x})\boldsymbol{\Gamma}_B \tag{23}$$

By comparing equation (25) with equation (17), we can obtain $\boldsymbol{F(x)}$ and $\boldsymbol{G(x)}$:

$$\begin{aligned}\boldsymbol{F}(\boldsymbol{x}) = \boldsymbol{L}_{\boldsymbol{f}}^2\boldsymbol{h}(\boldsymbol{x}) &= -\frac{1}{2}\boldsymbol{E}_1^T\hat{\boldsymbol{J}}^{-1}\boldsymbol{\omega}^{\times}\hat{\boldsymbol{J}}\boldsymbol{\omega} - N(\dot{\boldsymbol{q}})\boldsymbol{q} \\ \boldsymbol{G}(\boldsymbol{x}) = \boldsymbol{L}_{\boldsymbol{g}}\boldsymbol{L}_{\boldsymbol{f}}\boldsymbol{h}(\boldsymbol{x}) &= \frac{1}{2}\boldsymbol{E}_1^T\hat{\boldsymbol{J}}^{-1}\end{aligned} \tag{24}$$

And equation (23) can be rewritten as:

$$\ddot{\boldsymbol{y}} = \boldsymbol{F}(\boldsymbol{x}) + \boldsymbol{G}(\boldsymbol{x})\boldsymbol{\Gamma}_B = \boldsymbol{\nu} \tag{25}$$

We define the second derivatives of the outputs as the "virtual inputs", $\ddot{\boldsymbol{y}} = \boldsymbol{\nu} = [\nu_1 \quad \nu_2 \quad \nu_3 \quad \nu_4]^T$, a 4×1 input vector for the linearized system:

$$\frac{d}{dt}\boldsymbol{\xi} = \begin{bmatrix}\boldsymbol{0}_{4\times4} & \boldsymbol{I}_{4\times4} \\ \boldsymbol{0}_{4\times4} & \boldsymbol{0}_{4\times4}\end{bmatrix}\boldsymbol{\xi} + \begin{bmatrix}\boldsymbol{0}_{4\times4} \\ \boldsymbol{I}_{4\times4}\end{bmatrix}\boldsymbol{\nu} \tag{26}$$

where $\boldsymbol{\xi} = [\boldsymbol{y}^T \quad \dot{\boldsymbol{y}}^T]^T = [\boldsymbol{q}^T \quad \dot{\boldsymbol{q}}^T]^T$ is the 6×1 states vector of the linearized system.

Using the pseudoinverse of $\boldsymbol{E}_1^T\hat{\boldsymbol{J}}^{-1}$, we can express the control inputs in terms of the virtual inputs:

$$\boldsymbol{\Gamma}_B = (\boldsymbol{E}_1^T\hat{\boldsymbol{J}}^{-1})^{\dagger}(2\boldsymbol{\nu} + \boldsymbol{E}_1^T\hat{\boldsymbol{J}}^{-1}\boldsymbol{\omega}^{\times}\hat{\boldsymbol{J}}\boldsymbol{\omega} + 2(\dot{\boldsymbol{q}}^T\dot{\boldsymbol{q}})\boldsymbol{q}) \tag{27}$$

Since $\boldsymbol{E}_1^T\hat{\boldsymbol{J}}^{-1}$ is not a square matrix, we use the pseudoinverse of $\boldsymbol{G(x)}$. In the next subsection, we examine whether a singularity exists in this NDI formulation, as observed in previous studies [17,19–21].

4.1. Singularity Analtsis of the Matrix Inversion

The matrix $\boldsymbol{E}_1^T\hat{\boldsymbol{J}}^{-1}$ in Equation (27) is a 4×3 matrix. To determine whether a pseudoinverse exists, we examine its column rank. If the rank is 3, the pseudoinverse exists, and no singularity occurs during inversion. To show that $\boldsymbol{E}_1^T\hat{\boldsymbol{J}}^{-1}$ is full column rank, it is equivalent showing that the matrix $(\boldsymbol{E}_1^T\hat{\boldsymbol{J}}^{-1})^T(\boldsymbol{E}_1^T\hat{\boldsymbol{J}}^{-1})$ is full rank and invertible.

$$\begin{aligned}\big(\boldsymbol{E}_1^T\hat{\boldsymbol{J}}^{-1}\big)^T\big(\boldsymbol{E}_1^T\hat{\boldsymbol{J}}^{-1}\big) &= \hat{\boldsymbol{J}}^{-1}\boldsymbol{E}_1\boldsymbol{E}_1^T\hat{\boldsymbol{J}}^{-1} = \hat{\boldsymbol{J}}^{-2} \\ &= \begin{bmatrix}\frac{1}{J_1^2} & 0 & 0 \\ 0 & \frac{1}{J_2^2} & 0 \\ 0 & 0 & \frac{1}{J_3^2}\end{bmatrix}\end{aligned} \tag{28}$$

Since the result in equation (28) is a diagonal matrix and the moments of inertia of the principal axes are always positive, $\boldsymbol{E}_1^T\hat{\boldsymbol{J}}^{-1}$ is full column rank and its pseudoinverse exists.

 doi:10.20944/preprints202604.2045.v1

The pseudoinverse of $\boldsymbol{E}_1^T\hat{\boldsymbol{J}}^{-1}$ is referred to as a "left inverse" because it is a tall matrix. The inverse is provided below:

$$\begin{aligned}(\boldsymbol{E}_1^T\hat{\boldsymbol{J}}^{-1})^{\dagger} &= \left[(\boldsymbol{E}_1^T\hat{\boldsymbol{J}}^{-1})^T(\boldsymbol{E}_1^T\hat{\boldsymbol{J}}^{-1})\right]^{-1}(\boldsymbol{E}_1^T\hat{\boldsymbol{J}}^{-1})^T \\ &= \begin{bmatrix} -J_1q_1 & J_1q_0 & J_1q_3 & -J_1q_2 \\ -J_2q_2 & -J_2q_3 & J_2q_0 & J_2q_1 \\ -J_3q_3 & J_3q_2 & -J_3q_1 & J_3q_0 \end{bmatrix}\end{aligned} \tag{29}$$

In previous works [19,20] that derive the NDI formulation using a Newtonian mechanics approach, the counterpart matrix $\boldsymbol{G}(\boldsymbol{x})$ to be inverted has the form:

$$\boldsymbol{G}(\boldsymbol{x}) = \frac{1}{2}\begin{bmatrix} \frac{q_0}{J_1} & -\frac{q_3}{J_2} & \frac{q_2}{J_3} \\ \frac{q_3}{J_1} & \frac{q_0}{J_2} & -\frac{q_1}{J_3} \\ -\frac{q_2}{J_1} & \frac{q_1}{J_2} & \frac{q_0}{J_3} \end{bmatrix} \tag{30}$$

With its determinant

$$\det\big(\boldsymbol{G}(\boldsymbol{x})\big) = \frac{q_0}{8J_1J_2J_3} \tag{31}$$

The result shows a singularity at $q_0 = 0$, which leads to numerical instability when calculating the control torque.

In summary, the NDI formulation derived from the Lagrange mechanics approach can include both the vector and scalar parts of quaternions as outputs. Importantly, this approach does not exhibit the singularity reported in previous work, providing a robust foundation for controller design.

4.2. Linear Quadratic Tracking Controller

After the NDI formulation, a linear quadratic controller is designed to determine the virtual input in Equation (25). In Figure 1, the blue area represents the linearized equivalent system, and the LQ controller provides the virtual input $\boldsymbol{\nu}$ to control the output $\boldsymbol{y}$ and track the reference signal $\boldsymbol{y}_{ref}$.

A linear quadratic controller for attitude tracking is formulated to minimize the cost functional:

$$J = \int_0^{\infty} \left((\boldsymbol{\xi} - \boldsymbol{\xi}_{\boldsymbol{ref}})^T\boldsymbol{Q}(\boldsymbol{\xi} - \boldsymbol{\xi}_{\boldsymbol{ref}}) + \boldsymbol{\nu}^T\boldsymbol{R}\boldsymbol{\nu}\right) dt \tag{32}$$

and subject to the linearized dynamic system (26). $\boldsymbol{Q}$ and $\boldsymbol{R}$ are positive definite matrices representing the weighting matrices for the linear system's states and virtual inputs. The control input vector computed by the linear quadratic method takes the form: $\boldsymbol{\nu} = -\boldsymbol{K}\big(\boldsymbol{\xi} - \boldsymbol{\xi}_{\boldsymbol{ref}}\big) = -\boldsymbol{K}\boldsymbol{\xi} + \boldsymbol{r}$, where $\boldsymbol{K}$ is the state feedback gain and $\boldsymbol{r}$ is the feedforward term. [29]

The state feedback gain is obtained by solving the Riccati equation. In our case, it can be partitioned into two submatrices, $\boldsymbol{K} = \begin{bmatrix}\boldsymbol{K}_y & \boldsymbol{K}_{\dot{y}}\end{bmatrix}$, corresponding to their respective state variables. When tracking a desired attitude, $\boldsymbol{q}_d$, we set the reference siganl as $\boldsymbol{y}_{ref} = \boldsymbol{q}_d$, and the state vector at equilibrium point is $\xi_{ref} = [\boldsymbol{y}_{ref}^T \quad \boldsymbol{0}_{4\times1}^T]^T$. The feedforward term is then $\boldsymbol{r} = \boldsymbol{K}_y\boldsymbol{y}_{ref}$. To summarize, the virtual control input consists of both feedback and feedforward components, as shown below.

$$\boldsymbol{\nu} = -\begin{bmatrix}\boldsymbol{K}_y & \boldsymbol{K}_{\dot{y}}\end{bmatrix}\boldsymbol{\xi} + \boldsymbol{K}_y\boldsymbol{y}_{ref} \tag{33}$$

5. Nonlinear Disturbance Observer-Based Controller

Nonlinear systems often encounter unmodeled disturbances, which can significantly impact the performance of model-based controllers. These disturbances may originate from the external environment, parameter uncertainty, or unmodeled dynamics. Chen et al. [25] classified such disturbances as either matched or mismatched. In our application, external disturbances result from shifts in the center of gravity and the center of the spherical air-bearing, producing additional torque

 doi:10.20944/preprints202604.2045.v1

on the attitude control testbed. Because this disturbance acts through the same channel as the control torque, it is considered as a matched disturbance. The rotation dynamics with external disturbances can be represented as follows:

$$\begin{cases} \dot{\boldsymbol{x}} = \boldsymbol{f}(\boldsymbol{x}) + \boldsymbol{g_1}(\boldsymbol{x})\boldsymbol{u} + \boldsymbol{g_2}(\boldsymbol{x})\boldsymbol{d} \\ \boldsymbol{y} = \boldsymbol{h}(\boldsymbol{x}) \end{cases} \tag{34}$$

The state vector, $\boldsymbol{x} = [\boldsymbol{q} \quad \dot{\boldsymbol{q}}]$, matches the nonlinear system in equation (18). $\boldsymbol{g_1}(\boldsymbol{x})$ corresponds to the $\boldsymbol{g}(\boldsymbol{x})$ matrix in equation (20), while $\boldsymbol{g_2}(\boldsymbol{x})$ maps disturbances $\boldsymbol{d}$ into the state space. For matched disturbances, we have $\boldsymbol{g_1}(\boldsymbol{x}) = \boldsymbol{g_2}(\boldsymbol{x}) = \boldsymbol{g}(\boldsymbol{x})$.

In the DOBC framework, the controller and disturbance observer loops are designed independently. This separation principle enables the direct application of the NDI and LQ controller results from the previous section. We first introduce the DOBC framework to propose a nonlinear observer gain function based on the Lagrange equation of motion using quaternions, and then combine the control torque from the LQ controller with the estimated disturbance to obtain the final control inputs for the nonlinear system (36). The orange block in Figure 1 illustrates the disturbance observer structure. The estimated disturbance is fed forward to the control input through the triangular gain block β, located between the blue and orange blocks.

Chen et al. [25] reviewed various disturbance observers and their corresponding DOBCs, considering the characteristics of the target system and disturbances. For nonlinear systems with matched disturbances, they propose a nonlinear disturbance observer:

$$\begin{cases} \dot{\boldsymbol{z}} = -\boldsymbol{L}(\boldsymbol{x})\boldsymbol{g}(\boldsymbol{x})\boldsymbol{z} - \boldsymbol{L}(\boldsymbol{x})[\boldsymbol{g}(\boldsymbol{x})\boldsymbol{p}(\boldsymbol{x}) + \boldsymbol{f}(\boldsymbol{x}) + \boldsymbol{g}(\boldsymbol{x})\boldsymbol{u}] \\ \widehat{\boldsymbol{d}} = \boldsymbol{z} + \boldsymbol{p}(\boldsymbol{x}) \end{cases} \tag{35}$$

The observer output, $\widehat{\boldsymbol{d}}$ in the lower part of Equation (35), represents the estimated disturbance. It is calculated as the sum of the observer's internal states, $\boldsymbol{z}$, and a nonlinear function, $\boldsymbol{p}(\boldsymbol{x})$, which must be designed. The upper part of Equation (35) describes the dynamics of the internal states, which depend on the nonlinear system (36). The relationship between observer gain function $\boldsymbol{L}(\boldsymbol{x})$ and $\boldsymbol{p}(\boldsymbol{x})$ is given below:

$$\boldsymbol{L}(\boldsymbol{x}) = \frac{\partial \boldsymbol{p}(\boldsymbol{x})}{\partial \boldsymbol{x}} \tag{36}$$

The observer gain function $\boldsymbol{L}(\boldsymbol{x})$ should be chosen to ensure the asymptotic stability of the disturbance estimation error equation, defined as:

$$\dot{\boldsymbol{e}}_{\boldsymbol{d}}(t) + \boldsymbol{L}(\boldsymbol{x})\boldsymbol{g}(\boldsymbol{x})\boldsymbol{e}_d(t) = 0 \tag{37}$$

The disturbance estimation error is defined as the difference between the actual disturbance and its estimate, $\boldsymbol{e}_d = \boldsymbol{d} - \widehat{\boldsymbol{d}}$. Therefore, when designing the disturbance observer, we first determine $\boldsymbol{L}(\boldsymbol{x})$, then obtain $\boldsymbol{p}(\boldsymbol{x})$ by integrating $\boldsymbol{L}(\boldsymbol{x})$. The following subsection discusses the details of designing the observer gain function.

Equation (37) is a first-order ODE. If $\boldsymbol{L}(\boldsymbol{x})\boldsymbol{g}(\boldsymbol{x})$ is positive definite, the ODE is stable. The gain function can be defined as $\boldsymbol{L}(\boldsymbol{x}) = [\boldsymbol{L}_1 \quad \boldsymbol{L}_2]$, so $\boldsymbol{L}(\boldsymbol{x})\boldsymbol{g}(\boldsymbol{x}) = \boldsymbol{L}_1\boldsymbol{g}_u + \boldsymbol{L}_2\boldsymbol{g}_l$. Since $\boldsymbol{g}(\boldsymbol{x}) = [\boldsymbol{0}_{4\times3} \quad \frac{1}{2}\boldsymbol{E}_1^T\hat{\boldsymbol{J}}^{-1}]^T$, and $\boldsymbol{L}_1\boldsymbol{g}_u = \boldsymbol{0}$, equation (37) is equivalent to:

$$\dot{\boldsymbol{e}}_{\boldsymbol{d}}(t) + \boldsymbol{L}_2(\boldsymbol{x})\boldsymbol{g}_l(\boldsymbol{x})\boldsymbol{e}_d(t) = 0 \tag{38}$$

Therefore, we can design $\boldsymbol{L}_2$ first by setting $\boldsymbol{L}_2\boldsymbol{g}_l \succ 0$. To guarantee that $\boldsymbol{L}_2\boldsymbol{g}_l$ be positive definite, we can simply let it be an identity matrix multiplied by a positive-scalar gain K_{obs}. Learning that $\boldsymbol{g}_l = \frac{1}{2}\boldsymbol{E}_1^T\hat{\boldsymbol{J}}^{-1}$, and the property in Equation (6),we can set $\boldsymbol{L}_2 = K_{obs}\hat{\boldsymbol{J}}\boldsymbol{E}_1$ so that

$$\boldsymbol{L}_2(\boldsymbol{x})\boldsymbol{g}_l(\boldsymbol{x}) = \frac{1}{2}K_{obs}\hat{\boldsymbol{J}}\boldsymbol{E}_1\boldsymbol{E}_1^T\hat{\boldsymbol{J}}^{-1} = \frac{1}{2}K_{obs}\boldsymbol{I}_{3\times3} \tag{39}$$

It is clear from Equation (36) that $\boldsymbol{L}_2$ is the partial derivative of $\boldsymbol{p}(\boldsymbol{x})$ with respect to $\dot{\boldsymbol{q}}$. Expanding $\boldsymbol{L}_2$ yields:

 doi:10.20944/preprints202604.2045.v1

$$\boldsymbol{L}_2(\boldsymbol{x}) = \frac{\partial \boldsymbol{p}(\boldsymbol{x})}{\dot{\boldsymbol{q}}} = K_{obs}\begin{bmatrix} -J_1 q_1 & J_1 q_0 & J_1 q_3 & -J_1 q_2 \\ -J_2 q_2 & -J_2 q_3 & J_2 q_0 & J_2 q_1 \\ -J_3 q_3 & J_3 q_2 & -J_3 q_1 & J_3 q_0 \end{bmatrix} \tag{40}$$

The nonlinear function $\boldsymbol{p}(\boldsymbol{x})$ can be obtained by integrating $\boldsymbol{L}_2$ with respect to $\dot{\boldsymbol{q}}$. Assuming a zero constant of integration for simplicity, which leads to:

$$\boldsymbol{p}(\boldsymbol{x}) = K_{obs}\begin{bmatrix} J_1(-q_1\dot{q}_0 + q_0\dot{q}_1 + q_3\dot{q}_2 - q_2\dot{q}_3) \\ J_2(-q_2\dot{q}_0 - q_3\dot{q}_1 + q_0\dot{q}_2 + q_1\dot{q}_3) \\ J_3(-q_3\dot{q}_0 + q_2\dot{q}_1 - q_1\dot{q}_2 + q_0\dot{q}_3) \end{bmatrix} \tag{41}$$

And $\boldsymbol{L}_1$ can be derived by partially differentiating $\boldsymbol{p}(\boldsymbol{x})$ with respect to $\boldsymbol{q}$.

$$\boldsymbol{L}_1(\boldsymbol{x}) = \frac{\partial \boldsymbol{p}(\boldsymbol{x})}{\boldsymbol{q}} = K_{obs}\begin{bmatrix} J_1\dot{q}_1 & -J_1\dot{q}_0 & -J_1\dot{q}_3 & J_1\dot{q}_2 \\ J_2\dot{q}_2 & J_2\dot{q}_3 & -J_2\dot{q}_0 & -J_2\dot{q}_1 \\ J_3\dot{q}_3 & -J_3\dot{q}_2 & J_3\dot{q}_1 & -J_3\dot{q}_0 \end{bmatrix} = -K_{obs}\hat{\boldsymbol{J}}\dot{\boldsymbol{E}}_1 \tag{42}$$

While the condition $\boldsymbol{L}_1\boldsymbol{g}_u = \boldsymbol{0}$ does not affect Equation (37) and allows us to design $\boldsymbol{L}_2$ first, the $\dot{\boldsymbol{z}}$ dynamics in Equation (35) includes the term $\boldsymbol{L}(\boldsymbol{x})\boldsymbol{f}(\boldsymbol{x}) = \boldsymbol{L}_1\boldsymbol{f}_u + \boldsymbol{L}_2\boldsymbol{f}_l$. Since $\boldsymbol{f}_u \neq \boldsymbol{0}$, it is necessary to investigate the influence of $\boldsymbol{L}_1$on $\dot{\boldsymbol{z}}$. From the property described by Equation (9), it follows that:

$$\boldsymbol{L}_1\boldsymbol{f}_u = -K_{obs}\hat{\boldsymbol{J}}\dot{\boldsymbol{E}}_1\left(\frac{1}{2}\boldsymbol{E}^T\boldsymbol{w}\right) = -K_{obs}\hat{\boldsymbol{J}}\dot{\boldsymbol{E}}_1\dot{\boldsymbol{q}} = \boldsymbol{0}_{3\times 1} \tag{43}$$

Given that $\boldsymbol{L}_1$ has no influence on the dynamics of $\boldsymbol{z}$, as shown in Equation (45), the gain K_{obs} becomes negligible. Thus, the observer gain function $\boldsymbol{L}(\boldsymbol{x})$ is constructed as:

$$\boldsymbol{L}(\boldsymbol{x}) = [-\hat{\boldsymbol{J}}\dot{\boldsymbol{E}}_1 \quad K_{obs}\hat{\boldsymbol{J}}\boldsymbol{E}_1] \tag{44}$$

After determining $\boldsymbol{L}(\boldsymbol{x})$ and $\boldsymbol{p}(\boldsymbol{x})$, the estimated disturbance can be obtained from Equation (35). The system input $\boldsymbol{u}$ should not be taken directly from the control torque calculated by the NDI and LQ controller. Disturbance compensation is applied before the control torque is used in the nonlinear system:

$$\boldsymbol{u} = \boldsymbol{\Gamma}_{\boldsymbol{B}} + \boldsymbol{\beta}\hat{\boldsymbol{d}} \tag{45}$$

The β in the equation above is the disturbance compensation gain. Chen et al. [25] provided various methods for determining this gain. In the case of matched disturbances, where $\boldsymbol{g_1}(\boldsymbol{x}) = \boldsymbol{g_2}(\boldsymbol{x})$, the gain reduces to -1. Therefore, the control input $\boldsymbol{u}$ for the nonlinear system becomes:

$$\boldsymbol{u} = \boldsymbol{\Gamma}_{\boldsymbol{B}} - \hat{\boldsymbol{d}} \tag{46}$$

The performance of the NDI incorporated with the DOBC framework is evaluated through simulations in the next section.

6. Simulation Results

This section presents the simulation results utilized to validate the efficacy of the proposed NDI-DOBC methodology. We categorize the simulations into four cases. First, the attitude tracking control with the zero-crossing of the scalar component of quaternions is examined in an ideal condition, characterized by a diagonal moment of inertia matrix and the absence of external disturbance. To underscore the singular-free attributes of the proposed NDI framework, we adopt the moment of inertia matrix and initial, final conditions from previous work [11] and compare the simulation results. In the subsequent case, we adjust the moment of inertia matrix and add off-diagonal elements to test the robustness of the linear quadratic tracking controller in cooperation with the NDI framework.

The first case focuses on the general spacecraft static-to-static attitude control scenario, where the initial and target attitudes are denoted by $\boldsymbol{q}_I = [-0.742 \quad 0.2 \quad 0.4 \quad 0.5]^T$ and $\boldsymbol{q}_F = [0.447 \quad 0.6 \quad -0.2 \quad -0.632]^T$, respectively. In contrast, the second case considers a transition from an initially rotating state with an angular velocity of $\boldsymbol{\omega} = [0.5 \quad 0.5 \quad 0.5]^T\ rad/s$ to a static target attitude $\boldsymbol{q}_F$. The moment of inertia matrices for simulation case 1 and 2 are listed below: in case 1, we

 doi:10.20944/preprints202604.2045.v1

use a diagonal moment of inertia matrix, $\hat{\boldsymbol{J}}_d$, in the derivation of NDI and the simulation; while in case 2, the $\hat{\boldsymbol{J}}_d$ is used for NDI derivation, but the simulation is conducted with $\hat{\boldsymbol{J}}_1$, $\hat{\boldsymbol{J}}_2$ and $\hat{\boldsymbol{J}}_3$.

$$\hat{\boldsymbol{J}}_{\boldsymbol{d}} = \begin{bmatrix} 300 & 0 & 0 \\ 0 & 320 & 0 \\ 0 & 0 & 250 \end{bmatrix} \quad \hat{\boldsymbol{J}}_1 = \begin{bmatrix} 300 & -32 & 25 \\ -32 & 320 & -30 \\ 25 & -30 & 250 \end{bmatrix}$$

$$\hat{\boldsymbol{J}}_2 = \begin{bmatrix} 150 & -32 & 25 \\ -32 & 160 & -30 \\ 25 & -30 & 125 \end{bmatrix} \quad \hat{\boldsymbol{J}}_3 = \begin{bmatrix} 90 & -32 & 25 \\ -32 & 96 & -30 \\ 25 & -30 & 75 \end{bmatrix} \quad (\mathrm{kg \cdot m^2}) \tag{47}$$

The third simulation case introduces disturbances, with a focus on the attitude control testbed as the target. The disturbance is caused by the displacement of the center of gravity and the support of the air bearing, as illustrated in Figure 3. The gravitational force generates a moment that depends on the testbed's attitude. We use the DOBC to estimate and counteract the disturbance's impact. Given the constrained roll and pitch angles of the testbed, we define new initial and target conditions. Represented in Euler angles, the testbed transitions from an initial roll, pitch, and yaw of -5°, 10°, and 0° to a target of 0°, 0°, and 60°.

The fourth case considers both model mismatch and disturbance, reflecting the real scenario of the attitude control testbed. The testbed's moment of inertia matrix, $\hat{\boldsymbol{J}}_{true}$, is calculated using CAD software and applied to simulation cases 3 and 4. For testing robustness under model mismatch and disturbance, the NDI is assumed to have only the diagonal information of the elements of $\hat{\boldsymbol{J}}_{true}$.

$$\hat{\boldsymbol{J}}_{true} = \begin{bmatrix} 1.1932 & -0.0474 & 0 \\ -0.0474 & 1.116 & 0 \\ 0 & 0 & 1.0798 \end{bmatrix} \quad (\mathrm{kg \cdot m^2}) \tag{48}$$

6.1. Case 1: Zero Crossing of Quaternions

The simulation of quaternions is shown in Figure 4. The results are compared with those from Bang's work [11] , both of which utilize a linear controller alongside NDI. The scalar component of quaternions, q_0, crosses zero at around t=12.7 seconds in our simulation, indicated by a green dashed line; and at t=7.9 seconds in Bang's case, marked by a blue dashed line in Figure 4. We can see that Bang's controller experiences more oscillations than ours before reaching the desired attitude.

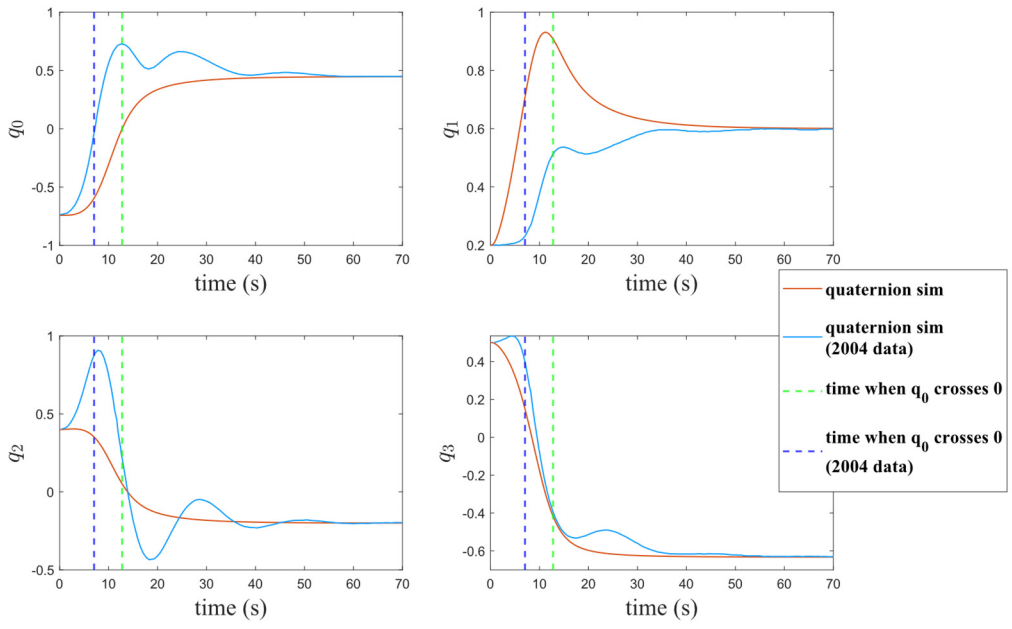

Figure 4. Comparison of quaternion simulation results between the proposed NDI and Bang's method [11]. The proposed method (red) outperforms Bang's method (blue) during the transient phase by providing a smooth convergence without oscillatory overshoots.

 doi:10.20944/preprints202604.2045.v1

The most significant difference between the two controllers is the derivatives of the control input, as shown in Figure 5. Bang's controller encounters the singularity of NDI, which causes rapid fluctuations in the control input. Its derivatives exceed 500, even with the modified gain to prevent the singularity. In contrast to the controller we proposed, the change in the control input remains smooth while q_0 crosses zero.

This simulation demonstrates that the proposed NDI formulation is free from singularities and can accurately track the desired attitude using a linear controller.

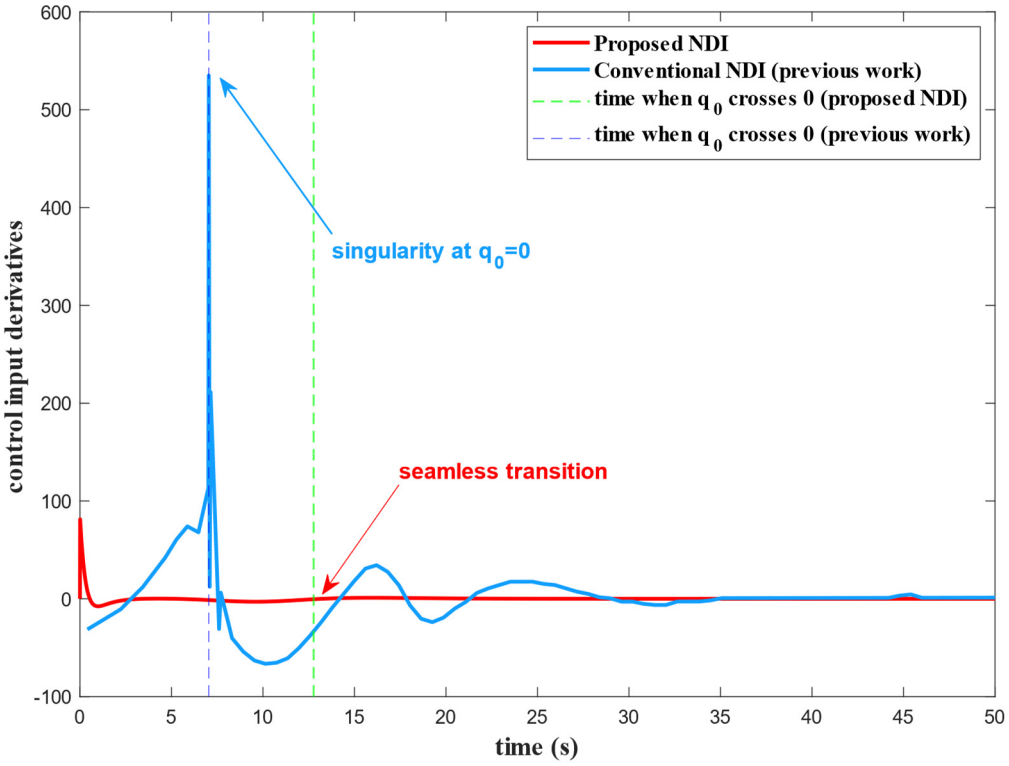

Figure 5. Comparison of control input derivatives between the proposed NDI and Bang's method [11]. While Bang's method (blue) suffers from severe numerical instability – evidenced by the massive spike when q_0 crosses zero – the proposed NDI method (red) successfully avoids this singularity, maintaining smooth and bounded control input derivatives.

6.2. Case 2: Robustness to Mismatched Moment of Inertia

In this case, we use the moment of inertia matrices $\hat{\boldsymbol{J}}_1$, $\hat{\boldsymbol{J}}_2$, and $\hat{\boldsymbol{J}}_3$ shown in Equation (47) for numerical simulation, but still adopt $\hat{\boldsymbol{J}}_d$ for deriving the NDI formulation. The cross-coupling terms and the decreasing diagonal terms in the moment of inertia matrices simulate the misalignment between principal axes and body-fixed axes and decreasing mass. The spacecraft is controlled by the LQ controller defined in Equation (32) with the weighting matrices $\boldsymbol{Q} = 10\boldsymbol{I}$ and $\boldsymbol{R} = \boldsymbol{I}$.

According to Newtonian rotational dynamics, the moment of inertia predominantly governs a system's transient rotational behavior. Consequently, to explicitly evaluate this effect, Case 2 – unlike Case 1 – is initialized with a non-zero angular velocity. As illustrated in Figure 6, although variations in the moment of inertia yield distinct transient paths, all trajectories successfully converge to the reference quaternions. These results effectively demonstrate the robustness of the combined NDI and LQ control scheme in handling model mismatches.

 doi:10.20944/preprints202604.2045.v1

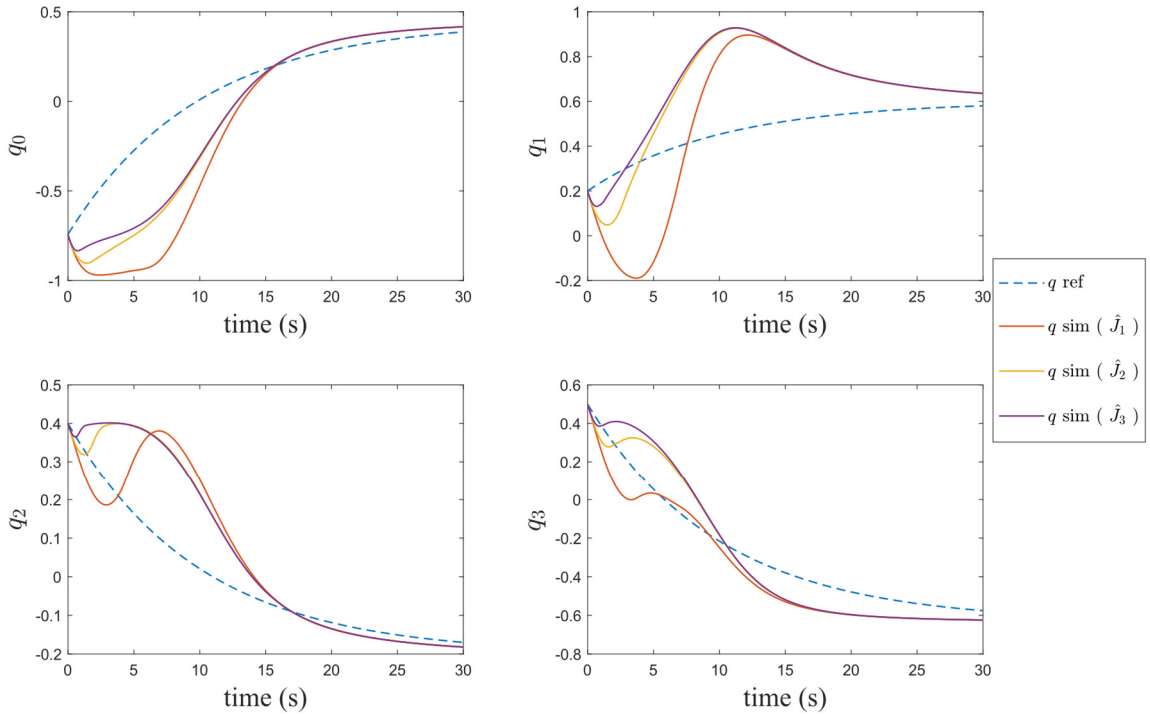

Figure 6. Quaternion simulation results under different mismatched moments of inertia. This simulation evaluates the system's performance under three distinct moment of inertia matrices ($\hat{J}_1$, $\hat{J}_2$, and $\hat{J}_3$), while the NDI is derived based on the nimonal matrix $\hat{J}_d$. As observed, although varying the inertia matrices yields different transient trajectories, the combined NDI and LQ controller successfully regulates the quaternions to the desired reference states. These results effectively validate the controller's robustness against inertial model mismatches.

6.3. Case 3: Robustness to External Disturbances

We introduce the DOBC derived in Section 5 to compensate for the influence of disturbances. The disturbance observer gain, K_{obs}, is tested with values of 1, 5, 10, and 20. Figure 7 shows the disturbance estimation error for the observer with different gains. Since the disturbances are related to the testbed's attitude, we use the error between the disturbance and the estimated one as the performance index for the observer. Figure 7 indicates that the larger the observer gain, the faster the estimation error converges.

Figure 8 and Figure 9 also show that the observer gain will significantly influence the performance of attitude control. It appears that all the estimation errors converge to zero in Figure 7, but biases still exist at the steady state. Take y-axis for example, the value of K_{obs} equals 1 (green line) and 20 (red line) are in the order of magnitude of 10^{-2} and 10^{-4}. These biases cause the poor performance of the green line in Figure 8 and Figure 9.

Although the red lines ($K_{obs} = 20$) have the fastest convergence time, this large gain not only induces oscillations in disturbance estimation but also affects attitude control. Therefore, we select $K_{obs} = 10$ as the observer gain for implementation.

 doi:10.20944/preprints202604.2045.v1

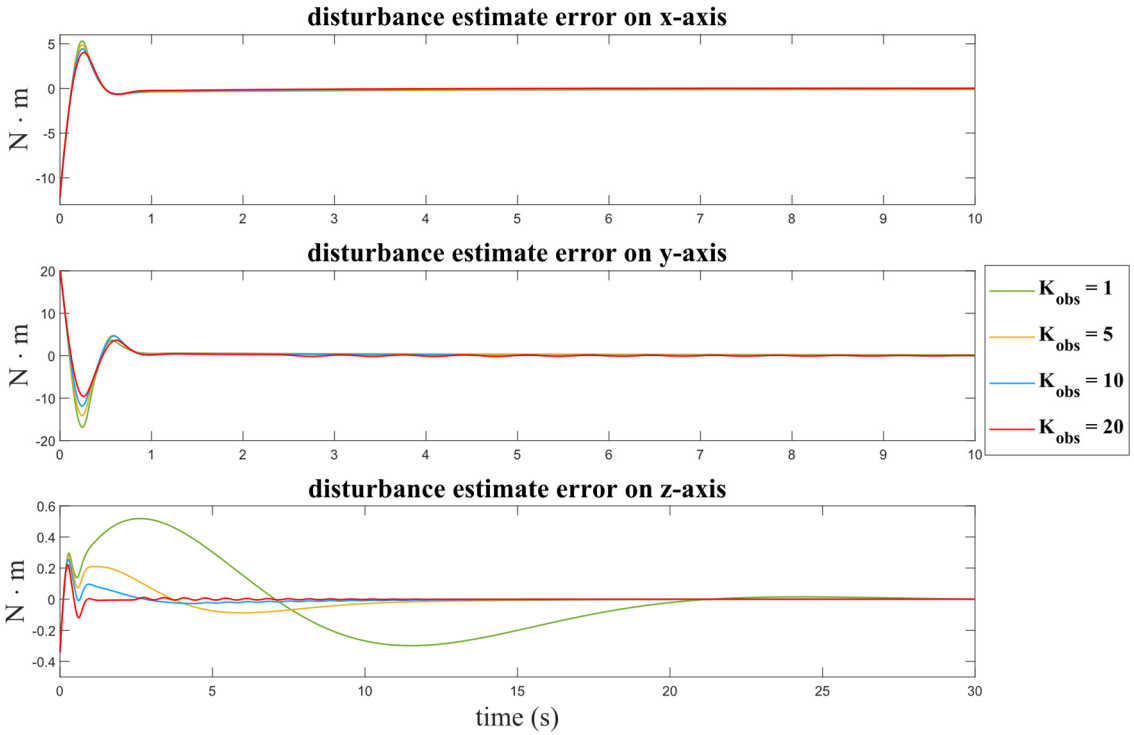

Figure 7. Disturbance estimation error with different observer gains. While a higher gain ($K_{obs} = 20$) yields a faster initial response, it introduces undesirable transient oscillations. Therefore, $K_{obs} = 10$ demonstrates the optimal balance, ensuring rapid convergence while maintaining transient smoothness.

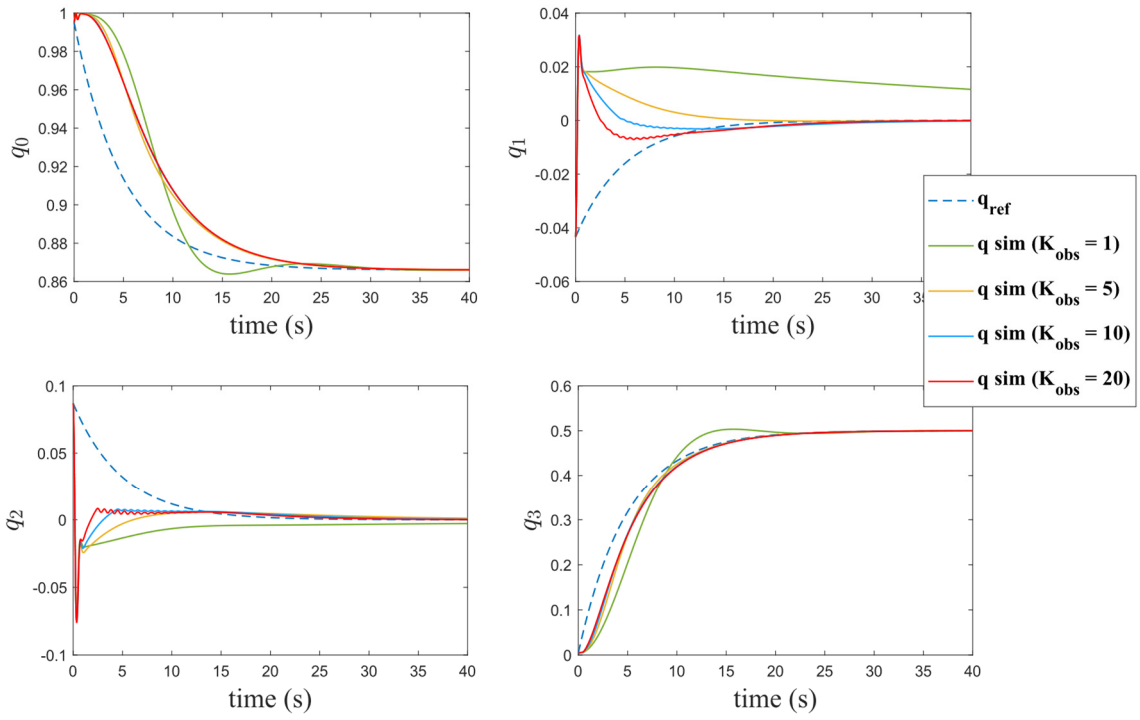

Figure 8. Quaternion simulation results with different observer gains. The trajectories indicate that although increasing K_{obs} improves the speed of convergence to the reference, it induces undesirable transient oscillations, which is particularly for $K_{obs} = 20$.

 doi:10.20944/preprints202604.2045.v1

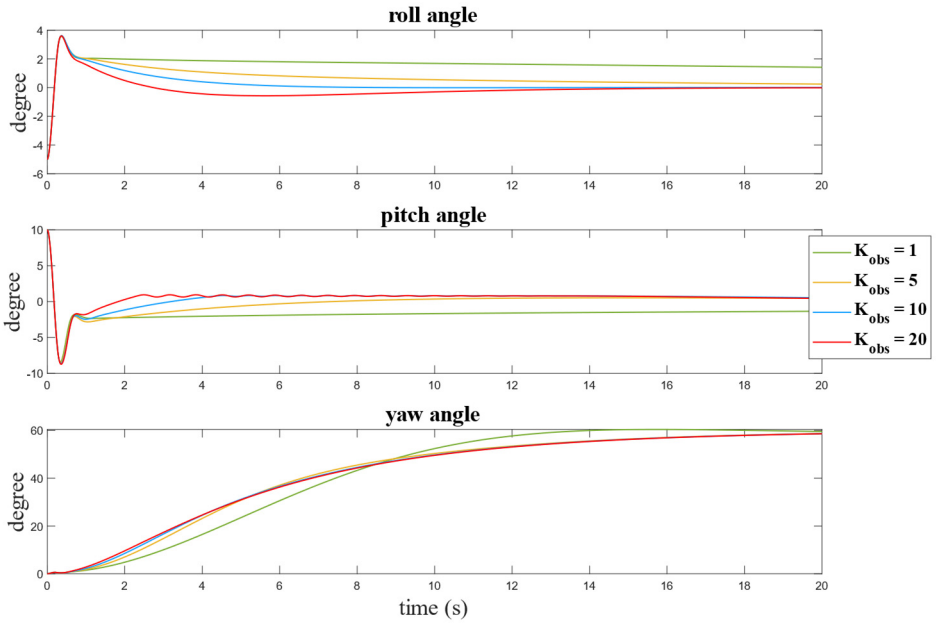

Figure 9. Euler angle representation of the simulation results from Figure 8. The plots demonstrate that both extreme gains yield suboptimal performance: $K_{obs} = 1$ fails to eliminate the steady-state error, whereas $K_{obs} = 20$ induces noticeable transient oscillations in the control response.

6.4. Case 4: Attitude Control with Both Model Mismatch and Disturbance

Finally, we adopt controller and observer gains designed from the two cases above and implement them in the scenario that contains both model mismatch and disturbance. The result is shown in Figure 10, where the yaw angle smoothly aligns with the desired heading. Meanwhile, the pitch and roll axes struggle to compensate for the disturbances caused by the initial pitch and roll angles. However, the DOBC rapidly takes effect to suppress these perturbations. Consequently, both axes achieve a smooth convergence to zero, while the yaw axis perfectly tracks the 60° target.

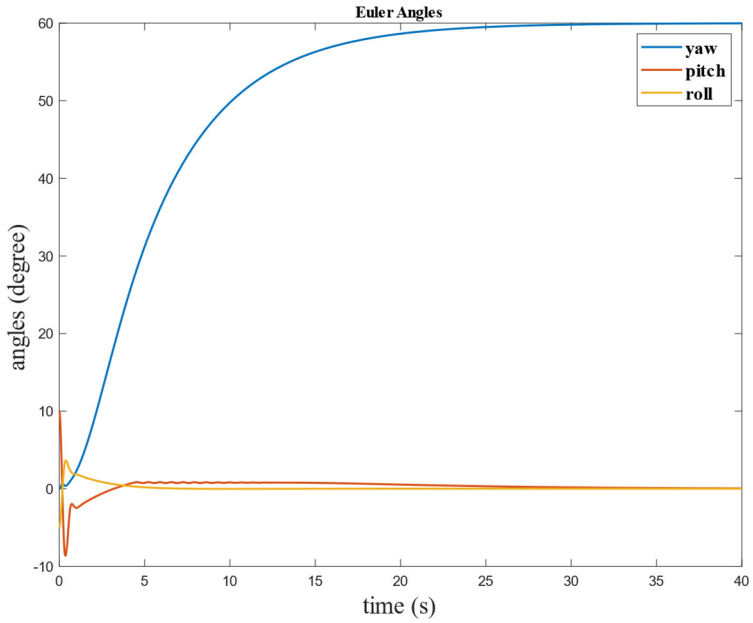

Figure 10. Euler angle response of the attitude testbed using the proposed NDI and DOBC framework. The results demonstrate that the controller successfully achieves the target attitude, effectively compensating for both model mismatches and external disturbances.

 doi:10.20944/preprints202604.2045.v1

7. Conclusion

This paper introduces a quaternion -based nonlinear dynamic inversion (NDI) framework incorporated with a disturbance-observer-based controller (DOBC) for attitude tracking control of a spacecraft. The NDI is derived using Lagrange mechanics of rotational motion in quaternion form, which avoids the singularity identified in previous studies. The singularity-free property for the condition $q_0 = 0$ is analytically proven and verified through simulations, ensuring the numerical stability of NDI.

To address model uncertainties and external disturbances, we design a linear quadratic (LQ) controller and a disturbance observer-based controller (DOBC). The nonlinear function and gain matrix of the DOBC are developed using the properties of quaternions to ensure convergence of the disturbance estimation error. The DOBC then compensates for the disturbances' effects on the control torque and enhances robustness.

Overall, the simulation results validate that the proposed control framework achieves precise attitude tracking while maintaining robust performance against uncertainties. To ensure practical relevance, the dynamic models for simulation Cases 3 and 4 are directly based on the actual attitude control testbed depicted in Figure 2. While this testbed emulates on-orbit attitude dynamics by providing a frictionless rotational environment, it is inevitably subject to gravity-induced torque disturbances. The results clearly demonstrate that the proposed NDI and DOBC framework successfully compensates for these physical disturbances, maintaining high-precision control. These promising outcomes highlight the approach's potential for real-world spacecraft applications and provide a solid foundation for future research in advanced attitude control strategies.

Author Contributions: Conceptuization, C.-T.S.; methodology, C.-T.S and C.-D.Y; software, C.-T.S.; validation, C.-T.S.; formal analysis, C.-T.S. and Y.-C.C.; investigation, C.-T.S.; resources, C.-T.S. and Y.-C.C; data curation, C.-T.S.; writing – original draft preparation, C.-T.S.; writing – review and editing, C.-T.S. and C.-D.Y; visualization, C.-T.S.; supervision, Y.-C.C.; project administration, Y.-C.C. All authors have read and agreed to the published version of the manuscript.

Funding: This work was supported by the National Science and Technology Council (NSTC) under Grant No. NSTC 108-2221-E-006-072-MY3 and 114-2221-E-006-070-MY3.

Data Availability Statement: The data presented in this study are available on request from the author.

Conflicts of Interest: The authors declare no conflicts of interest.

Abbreviations

The following abbreviations are used in this manuscript:

DOBC	Directory of open access journals
LQ	Linear quadratic
NDI	Nonlinear dynamic inversion

References

1. Wie, B., H. Weiss, and A. Arapostathis, *Quaternion feedback regulator for spacecraft eigenaxis rotations.* 1989.
2. Show, L.L., et al., *Spacecraft robust attitude tracking design: PID control approach.* Proceedings of the 2002 American Control Conference (IEEE Cat. No.CH37301), 2002.
3. Bang, H., M.-J. Tahk, and H.-D. Choi, *Large angle attitude control of spacecraft with actuator saturation.* Control Engineering Practice, 2003.
4. Yang, Y., *Analytic LQR Design for Spacecraft Control System Based on Quaternion Model.* 2012.
5. Kolosa, D., *Implementing a Linear Quadratic Spacecraft Attitude Control System.* 2015.
6. Enejor, E.U., et al., *Low Earth Orbit Satellite Attitude Stabilization Using Linear Quadratic Regulator.* European Journal of Electrical Engineering and Computer Science, 2023.

 doi:10.20944/preprints202604.2045.v1

7. Helmy, M., A. Hafez, and M. Ashry, *CubeSat attitude control via linear quadratic regulator (LQR).* Journal of Physics, 2023.
8. Corti, A., A. Dardanelli, and M. Lovera, *LPV methods for spacecraft control: An overview and two case studies.* American Control Conference, 2012.
9. Burgin, E., F. Biertümpfel, and H. Pfifer, *Linear Parameter Varying Controller Design For Satellite Attitude Control*.* IFAC-PapersOnLine, 2023.
10. Lo, S.-C. and Y.P. Chen, *Smooth Sliding-Mode Control for Spacecraft Attitude Tracking Maneuvers.* 1995.
11. Bang, H., J.-S. Lee, and Y.-J. Eun, *Nonlinear attitude control for a rigid spacecraft by feedback linearization.* KSME International Journal, 2004. **18**: p. 203 - 210.
12. Snell, S.A., D.F. Enns, and W.L. Garrard, *Nonlinear Inversion Flight Control for a Supermaneuverable Aircraft.* Journal of Guidance, Control, and Dynamics, 1992. **15**(4): p. 976–984.
13. Reiner, J., G. Balas, and W.L. Garrard, *Flight control design using robust dynamic inversion and time-scale separation.* Automatica, 1996.
14. Smith, P., *A SIMPLIFIED APPROACH TO NONLINEAR DYNAMIC INVERSION BASED FLIGHT CONTROL.* 1998.
15. Ito, D., et al., *Reentry Vehicle Flight Controls Design Guidelines: Dynamic Inversion.* 2002.
16. B, P.A., L.E. Briese, and K. Schnepper, *Guidance command generation and nonlinear dynamic inversion control for reusable launch vehicles.* Acta Astronautica, 2020.
17. Jensen, H.-C.B. and R. Wiśniewski, *Quaternion Feedback Control for Rigid-body Spacecraft.* 2001.
18. Banerjee, A. and R. Padhi, *Nonlinear Guidance and Autopilot Design for Lunar Soft Landing.* 2018.
19. Long, Y., et al., *Design and Quaternion-Based Attitude Control of the Omnicopter MAV Using Feedback Linearization.* 2012.
20. Navabi, M. and M.R.S.S.M.H. Hosseini, *Spacecraft quaternion based attitude input-output feedback linearization control using reaction wheels.* 2017 8th International Conference on Recent Advances in Space Technologies (RAST), 2017.
21. Bhargavapuri, M. and H. Parwana, *A Novel Quaternion-based Nonlinear Dynamic Inversion for Rigid Body Control.* 2021 Seventh Indian Control Conference (ICC), 2021.
22. Udwadia, F.E. and A. Schutte, *An Alternative Derivation of the Quaternion Equations of Motion for Rigid-Body Rotational Dynamics.* 2010.
23. Chen, W.H., *Nonlinear Disturbance Observer-Enhanced Dynamic Inversion Control of Missiles.* 2003.
24. Yang, J., W.H. Chen, and S. Li, *Non-linear disturbance observer-based robust control for systems with mismatched disturbances/uncertainties.* 2011.
25. Chen, W.H., et al., *Disturbance-Observer-Based Control and Related Methods—An Overview.* IEEE transactions on industrial electronics (1982. Print), 2016.
26. Schwartz, J.L., M.A. Peck, and C.D. Hall, *Historical review of air-bearing spacecraft simulators.* 2003.
27. Udwadia, F.E. and R.E. Kalaba, *A New Perspective on Constrained Motion.* Proceedings of the Royal Society of London Series A: Mathematical Physical and Engineering Sciences, 1992. **439**(1906): p. 407–410.
28. Sola, J., *Quaternion kinematics for the error-state Kalman filter.* arXiv preprint arXiv:1711.02508, 2017.
29. Franklin, G.F., J.D. Powell, and A. Emami-Naeini, *Feedback control of dynamic systems Gene F. Franklin, J. David Powell, Abbas Emami-Naeini.* 6th ed. 2010, Upper Saddle River, N.J. ;: Pearson Education.